IEEE Access
Multidisciplinary | Rapid Review | Open Access Journal

Received August 29, 2019, accepted October 2, 2019, date of publication October 7, 2019, date of current version October 21, 2019.

Digital Object Identifier 10.1109/ACCESS.2019.2946084

Inter-Numerology Interference for Beyond 5G

ABUU B. KIHERO[1], MUHAMMAD SOHAIB J. SOLAIJA[1], (Student Member, IEEE), AND HÜSEYIN ARSLAN[1,2], (Fellow, IEEE)

[1]Department of Electrical and Electronics Engineering, Istanbul Medipol University, 34810 Istanbul, Turkey
[2]Department of Electrical Engineering, University of South Florida, Tampa, FL 33620, USA

Corresponding author: Abuu B. Kihero (abkihero@st.medipol.edu.tr)

ABSTRACT Fifth generation (5G) radio access technology (RAT) is designed to flexibly serve multiple services with extremely diverse requirements. One of the steps taken toward fulfilling this vision of 5G-RAT is the introduction of multi-numerology concept, where multiple frame structures with different subcarrier spacings coexist in one frequency band. Though efficient in providing the required flexibility, this approach introduces a new kind of interference into the system known as inter-numerology interference (INI). In this study, a novel cyclic prefix (CP) insertion technique (referred to as common CP) for multi-numerology system is mathematically analyzed in terms of the INI problem and its extensive comparison with the conventional CP configuration (referred to as individual CP) standardized for the 5G multi-numerology systems is presented. An in-depth discussion of various critical issues concerning multi-numerology system such as frequency domain multiplexing, time domain symbol alignment, and orthogonality between subcarriers of different numerologies is presented in the light of both, individual and common CP configurations. The analyses reveal that common CP has an advantage of restructuring the INI pattern in the system in a manner that paves the way for developing better techniques of avoiding or minimizing INI in the future generations.

INDEX TERMS Interference analysis, inter-numerology interference, mixed numerologies, symbol alignment.

I. INTRODUCTION

A. BACKGROUND

The vision for fifth generation (5G) of wireless technology is much more than the mere evolution of broadband services. It envisages a more diverse network with seamless coverage, higher data rates, various services, massive connectivity, and significantly higher reliability than any earlier generation of mobile communication. As compared to the long-term evolution (LTE), 5G advertises a thousand-fold increase in data volume and number of connected devices per area, 100 times improvement in user data rates, reduction of energy consumption by a factor of 10 and decrease in latency by a factor of 5 [1]. These demands, when looked at simultaneously, seem improbable if not impossible to achieve, requiring multiple magnitudes of improvement in current technology and infrastructure.

As an approach to address these diverse service requirements, the standardization bodies, i.e., 3rd Generation Partnership Project (3GPP) and International Telecommunication Union Radiocommunication (ITU-R), have divided them into three different sets, one for each service, namely, enhanced mobile broadband (eMBB), ultra-reliable low latency communication (URLLC), and massive machine type communication (mMTC). eMBB prioritizes large bandwidth and high data rate, URLLC needs high reliability and low latency while mMTC necessitates low energy and bandwidth consumption and high coverage density [2]. It is important to keep in mind that this division of services is by no means thorough, and there are going to be various scenarios that do not fall completely within a single defined use-case [3].

In order to meet these diverse requirements of 5G services, there have been two primary candidate approaches proposed by researchers. First, proposition of new waveforms for 5G New Radio (5G-NR) and second, using different numerologies of the same parent waveform, orthogonal frequency division multiplexing (OFDM), where the term *numerology* refers to the different configurations of subcarrier spacing (Δf) and cyclic prefix (CP) duration of an OFDM symbol [4]. The first approach led to the proposition, analysis and comparison of various waveforms like filter bank multicarrier (FBMC), generalized frequency division multiplexing (GFDM), and universal filtered multi-carrier (UFMC). Several studies have compared these waveforms [5]–[7] and

The associate editor coordinating the review of this manuscript and approving it for publication was Jenny Mahoney.

TABLE 1. Numerology structures for data channels in 5G [10].

Parameters	Numerology options (μ)				
	0	**1**	**2**	**3**	**4**
Subcarrier Spacing (kHz)	15	30	60	120	240
OFDM Symbol Duration (µs)	66.67	33.33	16.67	8.33	4.17
CP Duration (µs)	4.69	2.34	4.17|1.17	0.58	0.29
Slot Duration (ms)	1	0.5	0.25	0.125	0.0625

it is the general consensus among the researchers that while each of these waveforms offers improvement over OFDM in some aspect, none of them can claim to address all requirements of 5G [8]. In addition to this, OFDM's maturity and the immense effort that is already put into its standardization for LTE led to it being selected as the waveform for 5G despite its CP overhead, frequency and time offset sensitivity, high peak-to-average power ratio (PAPR) and spectral regrowth issues [9]. Therefore, for 5G-NR, 3GPP has opted for the second approach, i.e., use of multiple numerologies of OFDM waveform. Table 1 gives a brief summary of the different numerologies present in the standard [10]. A total of five scalable numerology options are provided with the conventional LTE numerology (with $\Delta f = 15$ kHz) chosen as the fundamental numerology. By scalable we mean that all the standardized Δf's are 2^{μ} multiples of the fundamental LTE numerology (for $\mu = [0, 4]$). One basic reason for choosing this set of numerologies with scalable subcarrier spacing is to facilitate easy symbol alignment and clock synchronization in time domain, simplifying the implementation [2], [11].

It can be perceived intuitively how different numerologies can be used to meet the demands of each service class of 5G. For example, lower (in terms of Δf) numerologies are more suitable for mMTC, since they can support higher number of simultaneously connected devices within the same bandwidth and require lower power, intermediate numerologies are appropriate for eMBB which requires both, high data rate and significant bandwidth, and higher numerologies are more suitable for delay-sensitive applications pertaining to the URLLC service due to their shorter symbol duration. It is important to note that selection of numerologies does not depend solely on the service to be supported. Other factors such as cell size, time variation of the channel, delay spread, frequency band of operation, etc., also need to be taken into consideration in picking a numerology [12].

B. INTER-NUMEROLOGY INTERFERENCE AND THE STATE OF THE ART

While the use of multiple numerologies is essential in providing the necessary flexibility required for the diverse services, it introduces a non-orthogonality into the system which in turn causes interference between the multiplexed numerologies [2], [4], [12]–[14]. This new form of interference is referred to as inter-numerology interference (INI). Apart from causing the loss of orthogonality among subcarriers of different numerologies in frequency domain, mixed numerologies also cause difficulty in achieving symbol alignment in time domain. With the same sampling rate, an OFDM symbol of one numerology does not perfectly align with the symbol of another numerology, which makes synchronization within the frame difficult. However, with the scalable numerology design of 5G, symbol duration of one numerology is always an integer multiple of the symbol duration of another numerology (see Fig. 2). Therefore, multi-numerology symbols can be perfectly aligned over the so called least common multiplier symbol duration (T_{LCM}) as discussed in [11], [13], [15], [16].

In order to make intelligent use of the multi-numerology concept introduced by 5G-NR, an in-depth analysis and understanding of INI is inevitable. Researchers have already taken a step toward describing INI in detail and identifying various factors contributing to it. For instance, [4], [13] and [17] provide more generic analyses of INI for subband filtered multi-carrier (SFMC), windowed-OFDM and FBMC waveforms, respectively, and include an approximate INI analytical model for a special case of CP-OFDM waveform. Apart from the subcarrier spacing difference between adjacent numerologies, other factors such as channel response of the victim numerology, number of subcarriers in each numerology, power offset and amount of guard band (GB) between the numerologies, as well as windowing/filtering operations are found to have significant impact on the amount of INI suffered by the system [4], [13], [15]. In addition to analysis of the INI problem, some studies have already gone further and proposed techniques and algorithms to minimize the effect of INI. For instance, a study in [18] tries to optimize the guards in time and frequency domains to minimize INI while keeping in view the users' requirements and their power offset. The study in [19] heuristically discusses a power offset based scheduling technique in multi-numerology systems to minimize INI experienced by edge subcarriers of the multiplexed numerologies. Authors in [20] propose a transceiver design that takes advantage of the interference pattern to minimize variance of the interfering energy in the multi-numerology system. Additionally, some of the traditional techniques such as GB allocation, windowing, and filtering are also considered to be efficient ways of minimizing INI [4], [13], [21].

C. CONTRIBUTION OF THE PAPER

In our preliminary study [15], two different approaches of achieving symbol alignment over T_{LCM} duration, namely individual CP and common CP, are presented. The individual CP refers to the conventional CP configuration where a CP is attached to each OFDM symbol prior to transmission, as standardized for LTE and 5G systems. Common CP, on the other hand, is a relatively new CP configuration technique where one CP is used to protect multiple OFDM symbols against channel impairments [15], [22]–[25]. An in-depth analysis of the common CP configuration and its advantages over the individual CP in terms of inter symbol interference (ISI), inter carrier interference (ICI), spectral efficiency and

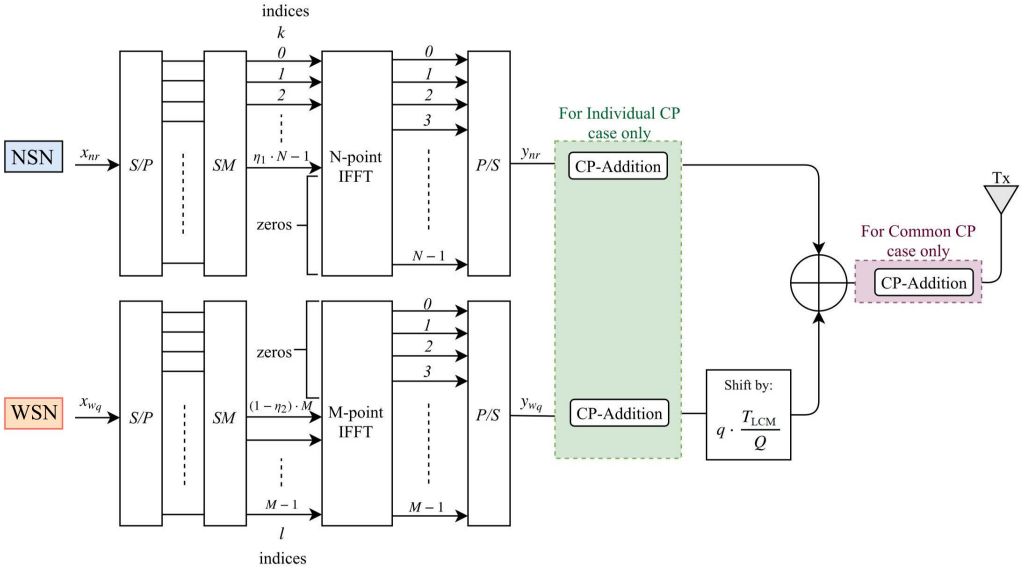

FIGURE 1. Downlink multi-numerology implementation at the transmitter.

complexity is presented in [24]. While 5G standard has limited itself to the use of conventional CP, it is important to look for alternative symbol alignment techniques that can provide additional flexibility in future networks. Armed with this motivation and the promise of common CP configuration, we extend the work presented in [15].

In [15], we briefly showed (through simulation) that utilization of the common CP can restructure the INI distribution in the system such that it opens doors for developing better techniques of avoiding or minimizing INI. Building on top of it, this paper provides an extensive theoretical and simulation analyses of the common CP in terms of INI and its thorough comparison with the conventional individual CP configuration. With the presented analysis, areas where INI can be controlled/minimized or even exploited to enhance performance of the systems are highlighted.

The rest of this paper is organized as follows. Section II discusses the downlink system model used for implementation of multi-numerology system and its mathematical formulation in both, frequency and time domains. Sections III and IV give detailed analytical derivations of the INI patterns for the individual and common CP configurations, respectively. Numerical analysis and insights derived from the observed results are discussed in Section V. Section VI finally concludes the paper.

II. SYSTEM MODEL

A. FREQUENCY DOMAIN

Let us consider a multi-numerology system with system bandwidth B shared between two users. Active subcarriers of the two users are assumed to utilize the bandwidth with the ratio η_1 and η_2, where $\eta_1 + \eta_2 = 1$ (i.e., no GB between the two numerologies is considered). For simplicity and numerical tractability of the analysis, only two users utilizing numerology-1 and numerology-2, respectively are considered in this model. However, the analysis developed herein can be applied to any number of multiplexed numerologies by considering one pair of numerologies at a time. Let the two numerologies utilize subcarrier spacing Δf_1 (narrow subcarrier spacing) and Δf_2 (wide subcarrier spacing), respectively. Throughout the paper we will refer to the first numerology with narrow subcarrier spacing as NSN, and to the second with wide subcarrier spacing as WSN. Abiding by the 5G standards, the ratio $\Delta f_2/\Delta f_1 = Q$ is always an integer power of 2. Note that $Q = 1$ refers to the case in which the two users are using the same numerology.

Fig. 1 illustrates the downlink implementation of the multi-numerology frequency-domain subcarriers multiplexing, time-domain symbol alignment, and creation of the composite signal for the transmission. The model employs subcarrier mapping (SM) blocks right after serial-to-parallel (S/P) blocks for properly arranging NSN and WSN subcarriers according to their specified portions of the spectrum. The SM blocks implement the localized subcarrier mapping technique whose output can be expressed as

$$X_{\mathrm{nr}}(k) = \begin{cases} x_{\mathrm{nr}}(k), & 0 \le k \le \eta_1 N - 1 \\ 0, & \eta_1 N \le k \le N - 1, \end{cases} \tag{1}$$

and

$$X_{\mathrm{w}}(l) = \begin{cases} 0, & 0 \le l \le (1-\eta_2)M - 1 \\ x_{\mathrm{w}}(l), & (1-\eta_2)M \le l \le M - 1, \end{cases} \tag{2}$$

where, N and M are fast Fourier transform (FFT)/inverse fast Fourier transform (IFFT) sizes of NSN and WSN respectively, such that $N = Q \times M$. $X_{\mathrm{nr}}(k)$ and $X_{\mathrm{w}}(l)$ are complex modulated symbols on k^{th} and l^{th} subcarriers of NSN and WSN, respectively, after SM.

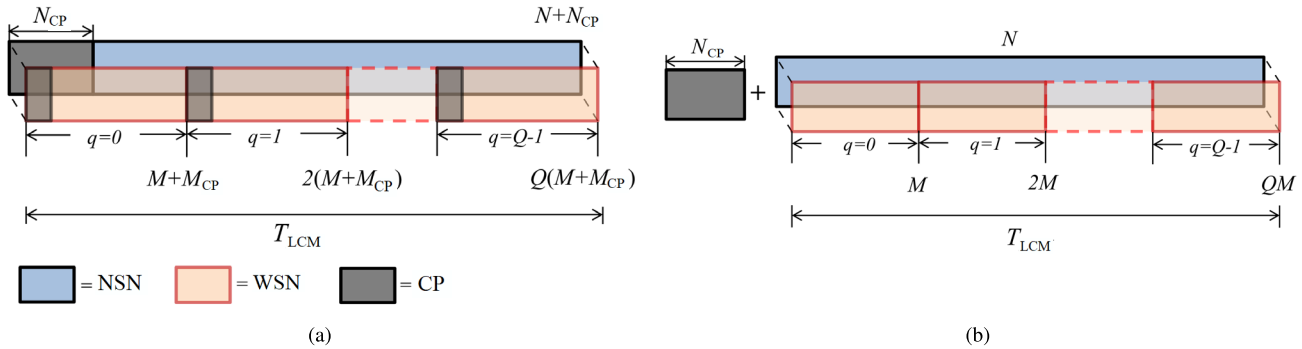

FIGURE 2. Multi-numerology symbol alignment over *LCM* symbol duration. (a) Individual CP case. (b) Common CP case.

B. TIME DOMAIN

The output of the IFFT blocks in Fig. 1 are time-domain symbols y_{nr} and y_{w} of NSN and WSN respectively, and they are given by

$$y_{\text{nr}}(n) = \text{IFFT}\{X_{\text{nr}}\}|_{\text{N-point}} = \frac{1}{\sqrt{N}} \sum_{k=0}^{\eta_1 N-1} X_{\text{nr}}(k) e^{j2\pi nk/N}, \quad \text{for} \quad 0 \le n \le N-1, \tag{3}$$

and

$$y_{\text{w}}(m) = \text{IFFT}\{X_{\text{w}}\}|_{\text{M-point}} = \frac{1}{\sqrt{M}} \sum_{l=\eta_1 M}^{M-1} X_{\text{w}}(l) e^{j2\pi ml/M}, \quad \text{for} \quad 0 \le m \le M-1. \tag{4}$$

If we are to observe the WSN subcarriers with the granularity of the NSN subcarriers, the l-indices of active subcarriers of WSN in (2) can be defined as $l = \eta_1 M + k/Q$ for $\{0 \le k \le \eta_2 N - 1 : k/Q \in \mathbb{Z}\}$. Consequently, (4) can be rewritten as

$$y_{\text{w}}(m) = \frac{1}{\sqrt{M}} \sum_{k=0}^{\eta_2 N-1} X_{\text{w}}(\eta_1 M + k/Q) e^{\frac{j2\pi}{N} m(k+\eta_1 N)}, \quad \text{for} \quad 0 \le m \le M-1. \tag{5}$$

As briefly explained in the introduction, the symbol alignment issue in the multi-numerology system is overcome when the multiplexed numerologies are integer multiples of one another. For instance, subcarrier spacing $\Delta f_2 = Q \times \Delta f_1$ implies that the symbol durations T_1 and T_2 are also related by $T_1 = Q \times T_2$, which means that Q-concatenated symbols of WSN can be perfectly aligned with one symbol of NSN as shown in Fig. 2. This gives rise to the concept of multi-numerology symbol alignment over T_{LCM} duration as mentioned earlier. T_{LCM} is always equal to the symbol duration of the numerology with the smallest Δf in a given system. With the exception of extended CP option for the numerology with $\Delta f = 60$ kHz, all standardized numerologies use the same CP ratio, which guarantees that the multi-numerology symbol alignment over T_{LCM} duration holds even after CP addition to the symbols. As we have mentioned before, in this study individual CP and common CP approaches of achieving multi-numerology symbol alignment are investigated.

1) INDIVIDUAL CP

The individual CP configuration is shown in Fig. 2(a). It is the conventional approach where CP is added to each of the Q symbols of WSN before concatenating them. Let N_{CP} and M_{CP} be the CP-sizes for NSN and WSN respectively, where $N_{\text{CP}} = Q \times M_{\text{CP}}$. After CP addition to each symbol, the ranges of indices n and m in (3) and (5) are redefined to $-N_{\text{CP}} \le n \le N-1$, and $-M_{\text{CP}} \le m \le M-1$, respectively. The Q-concatenated symbols of WSN with the individual CP (denoted by $y^I_{\text{w}_c}$) can be modeled as an M-point periodic extension of y_{w}, given as

$$y^I_{\text{w}_c} = \sum_{q=0}^{Q-1} y_{\text{w}_q}(m - q(M + M_{\text{CP}})), \tag{6}$$

where q is the WSN symbol index within T_{LCM} duration. Now, y_{nr} and $y^I_{\text{w}_c}$ are summed up to form a composite signal y of the two numerologies for transmission [16], given as

$$y = y_{\text{nr}} + y^I_{\text{w}_c}. \tag{7}$$

2) COMMON CP

In this approach all Q concatenated WSN symbols are protected by only one CP of length $Q \times M_{\text{CP}} (= N_{\text{CP}})$ as shown in Fig. 2(b). This approach is motivated by the concept of multi-symbols encapsulated OFDM (MSE-OFDM) studied in [22]–[24]. As reported in Table 1, CP size decreases with an increase in the subcarrier spacing. In case of a doubly dispersive channel, we do not have the flexibility to utilize larger subcarrier spacing and larger CP duration simultaneously to overcome ICI and ISI respectively. Common CP configuration provides a solution to this dilemma by allowing us to use larger subcarrier spacing and yet have larger CP duration to contain the ISI without compromising the spectral efficiency and receiver complexity [24]. In another study, authors have used common CP configuration to enhance performance of the multi-numerology based non-orthogonal multiple access (NOMA) systems [25]. Although common

CP configuration has exhibited better performance compared to the conventional individual CP structure in some scenarios, its INI performance is not yet well investigated. It should be understood that a modified frequency domain equalization technique has to be used at the receiver when common CP is utilized. Details concerning this equalization process can be found in [22] and [24].

Now, with the common CP, the Q-concatenated symbols of WSN (denoted by $y^C_{\mathrm{w}_c}$) can be given as

$$y^C_{\mathrm{w}_c} = \sum_{q=0}^{Q-1} y_{\mathrm{w}_q}(m - N_{\mathrm{CP}} - qM), \tag{8}$$

and the transmitted signal y is given by

$$y = y_{\mathrm{nr}} + y^C_{\mathrm{w}_c}. \tag{9}$$

Let us assume that the transmitted signal passes through a D-tap time varying multipath channel with its discrete channel impulse response (CIR) given by

$$h(m) = \sum_{d=0}^{D-1} \gamma_d(m)\delta(m - \tau_d), \tag{10}$$

where τ_d and γ_d are the propagation delay (in samples) and complex amplitude associated with the d^{th} tap, respectively. $\delta(\cdot)$ is the Dirac delta function that models the propagation delay of each tap. The received signal s is then expressed as

$$s(r) = \sum_{d=0}^{D-1} \gamma_d(r)y(r - \tau_d), \tag{11}$$

where additive channel noise is ignored.

In this analysis, we assume that a proper choice of numerology is made such that neither NSN nor WSN subcarriers are affected by ICI. Furthermore, we consider that N_{CP} and M_{CP} are larger than their respective targeted maximum excess delays such that both numerologies are not affected by ISI [26]. Therefore, only INI is expected in the system.

III. INTER-NUMEROLOGY INTERFERENCE ANALYSIS FOR INDIVIDUAL CP CONFIGURATION

A. INI FROM WSN TO NSN

At the receiver of the NSN user, N_{CP}-sized CP is removed and the time-domain received signal is transformed to the frequency domain for channel equalization and data detection processes. The N-point FFT of the received signal is taken as follows

$$S(v) = \mathrm{FFT}\{s(r)\}|_{\text{N-point}} = H^{\mathrm{NSN}}(v) \times Y(v), \tag{12}$$

for $0 \le v \le \eta_1 \times N - 1$, where v represents indices of the desired subcarriers of NSN, and $H^{\mathrm{NSN}}(v)$ denotes the channel frequency response (CFR) at v^{th} subcarrier, defined as

$$H^{\mathrm{NSN}}(v) = \sum_{d=0}^{D-1} \gamma_d^{\mathrm{NSN}}(v)\mathrm{e}^{-\frac{j2\pi}{N}v\tau_d}. \tag{13}$$

Y is the FFT of the composite transmitted signal y, given as

$$Y(v) = \frac{1}{\sqrt{N}} \sum_{r=N_{\mathrm{CP}}}^{N+N_{\mathrm{CP}}-1} y(r)\mathrm{e}^{-\frac{j2\pi}{N}rv}. \tag{14}$$

Since y is composed of the signals of the two multiplexed numerologies, Y will then consist of the desired symbols (Y_{des}) of NSN as well as the interference (Y_{INI}) it receive from sidelobes of the WSN subcarriers. So, (12) becomes

$$S(v) = H^{\mathrm{NSN}}(v) \times [Y_{\mathrm{des}}(v) + Y_{\mathrm{INI}}(v)]. \tag{15}$$

Since we have considered the flat fading sub-channel condition for each subcarrier, the channel effect in (15) can be completely compensated by using the conventional one-tap frequency domain equalization.

By using (14), (7), and (6), we can express the interference $Y_{\mathrm{INI}}(v)$ from WSN to v^{th} subcarrier of NSN as

$$Y_{\mathrm{INI}}(v) = \frac{1}{\sqrt{N}} \sum_{r=N_{\mathrm{CP}}}^{M+M_{\mathrm{CP}}-1} \sum_{q=0}^{Q-1} y_{\mathrm{w}_q}(r - q(M + M_{\mathrm{CP}})) \times \mathrm{e}^{-\frac{j2\pi}{N}v(r-q(M+M_{\mathrm{CP}}))}. \tag{16}$$

Note that among the Q concatenated symbols of WSN, only the first symbol (i.e., $q = 0$) overlaps with the CP portion of the NSN symbol. Therefore, due to the CP removal at the NSN receiver, we can write

$$Y_{\mathrm{INI}}(v) = \frac{1}{\sqrt{N}}\Bigg[\sum_{r=N_{\mathrm{CP}}}^{M+M_{\mathrm{CP}}-1} y_{\mathrm{w}_0}(r)\mathrm{e}^{-\frac{j2\pi}{N}rv} + \sum_{r=0}^{M+M_{\mathrm{CP}}-1} \sum_{q=1}^{Q-1} y_{\mathrm{w}_q}(r - q(M + M_{\mathrm{CP}})) \times \mathrm{e}^{-\frac{j2\pi}{N}v(r-q(M+M_{\mathrm{CP}}))}\Bigg]. \tag{17}$$

Further simplification of (17) is shown in Appendix A. Now, by substituting (36) and (37) from Appendix A into (17), we find the INI power $I_{\mathrm{NSN}}(k, v)$ from the k^{th} subcarrier of WSN to the v^{th} subcarrier of NSN as

$$I_{\mathrm{NSN}}(k, v) = |Y_{\mathrm{INI}}(k, v)|^2 = \frac{\rho^{\mathrm{WSN}}(k)}{N \times M}\Psi(k, v), \quad \text{for} \quad 0 \le v \le \eta_1 N - 1 \quad \text{and} \quad \{0 \le k \le \eta_2 N - 1 : k/Q \in \mathbb{Z}\}, \tag{18}$$

where

$$\Psi(k, v) = \frac{\left|\sin\left[\frac{\pi}{Q}\left(1 + (1 - Q)\mathrm{CP}_R\right)(k - v)\right]\right|^2}{\left|\sin\left[\frac{\pi}{N}(k - v + \eta_1 N)\right]\right|^2} + (Q - 1) \times \frac{\left|\sin\left[\frac{\pi}{Q}(1 + \mathrm{CP}_R)(k - v)\right]\right|^2}{\left|\sin\left[\frac{\pi}{N}(k - v + \eta_1 N)\right]\right|^2},$$

$\rho^{\mathrm{WSN}}(k) = |X_{\mathrm{w}}(\eta_2 M + k/Q)|^2$ is the WSN subcarrier power, and $\mathrm{CP}_R = N_{\mathrm{CP}}/N = M_{\mathrm{CP}}/M$ is the CP ratio employed by the the system. The term $k - v + \eta_1 N$ is the spectral distance between the interfering subcarrier at $k + \eta_1 N$ and the victim subcarrier at v. Note that when $Q = 1$, i.e., the system comprises of a single numerology, the INI power in (18) becomes zero as expected. Signal-to-interference ratio performance of the v^{th} subcarrier of NSN due to $I_{\mathrm{NSN}}(k, v)$ can be calculated as

$$\begin{aligned}\mathrm{SIR}_{\mathrm{NSN}}(v) &= \frac{\rho^{\mathrm{NSN}}(v)}{\sum_{k=0}^{\eta_2 N-1} I_{\mathrm{NSN}}(k, v)} \\ &= \frac{N \times M \times \rho^{\mathrm{NSN}}(v)}{\sum_{k=0}^{\eta_2 N-1} \rho^{\mathrm{WSN}}(k)\Psi(k, v)},\end{aligned} \tag{19}$$

where $\rho^{\mathrm{NSN}}(v) = |X_{\mathrm{nr}}(v)|^2$ is the NSN subcarrier power.

B. INI FROM NSN TO WSN

Again, we consider $s(r)$ in (11) as the received signal at WSN receiver. To demodulate the q^{th} symbol out of Q-concatenated symbols of WSN, the receiver captures $s(r - q(M + M_{\mathrm{CP}}))$ portion of the received signal, where $0 \le r \le M + M_{\mathrm{CP}} - 1$, such that

$$s(r - q(M + M_{\mathrm{CP}})) = y_{\mathrm{w}_q}(r) + y_{\mathrm{nr}}(r - q(M + M_{\mathrm{CP}})), \tag{20}$$

where $y_{\mathrm{nr}}(r - q(M + M_{\mathrm{CP}}))$ is the portion of the NSN symbol added to the q^{th} symbol of WSN during creation of the composite signal at the transmitter. M-point FFT process at the WSN receiver results in

$$\begin{aligned}S(v) &= \mathrm{FFT}\{s(r - q(M + M_{\mathrm{CP}}))\}|_{\text{M-point}} \\ &= H^{\mathrm{WSN}}(v)[Y_{\mathrm{des}}(v) + Y_{\mathrm{INI}}(v)],\end{aligned} \tag{21}$$

where $H^{\mathrm{WSN}}(v)$ is the CFR at the v^{th} subcarrier of WSN user given as

$$H^{\mathrm{WSN}}(v) = \sum_{d=0}^{D-1} \gamma_d^{\mathrm{WSN}}(v) \mathrm{e}^{-\frac{j2\pi v \tau_d}{M}}. \tag{22}$$

Recalling the localized subcarrier mapping technique implemented at the transmitter, the indices v of the WSN subcarriers to be detected can be expressed as $v = \eta_2 M + p/Q$, where $\{0 \le p \le \eta_2 N - 1 : p/Q \in \mathbb{Z}\}$. We can thus write (21) as

$$\begin{aligned}S(\eta_1 M + p/Q) = H^{\mathrm{WSN}}(\eta_1 M + p/Q)\Big[&Y_{\mathrm{des}}(\eta_1 M + p/Q) \\ &+ Y_{\mathrm{INI}}(\eta_1 M + p/Q)\Big].\end{aligned} \tag{23}$$

Again, considering perfect channel equalization at the receiver, we can get rid of the channel effect H^{WSN} in (23).

Now, we can find the interference Y_{INI} from NSN to WSN as

$$\begin{aligned}&Y_{\mathrm{INI}}(\eta_1 M + p/Q) \\ &= \frac{1}{\sqrt{M}} \sum_{r=M_{\mathrm{CP}}}^{M+M_{\mathrm{CP}}-1} y_{\mathrm{nr}}(r - q(M + M_{\mathrm{CP}})) \mathrm{e}^{-\frac{j2\pi}{M} r(\eta_1 M + p/Q)} \\ &= \frac{1}{\sqrt{M}} \sum_{r=0}^{M-1} y_{\mathrm{nr}}(r + M_{\mathrm{CP}} - q(M + M_{\mathrm{CP}})) \\ &\quad \times \mathrm{e}^{-\frac{j2\pi}{M}(r + M_{\mathrm{CP}})(\eta_1 M + p/Q)}.\end{aligned} \tag{24}$$

(24) is simplified in Appendix B and (38) is obtained. Now, by using (23) and (38) the INI power, $I_{\mathrm{WSN}}(k, p)$ from k^{th} subcarrier of NSN to the p^{th} subcarrier of WSN can be given as

$$\begin{aligned}I_{\mathrm{WSN}}(k, p) = |Y_{\mathrm{INI}}(k, \eta_1 M + p/Q)|^2 = \frac{\rho^{\mathrm{NSN}}(k)}{N \times M} |\xi(k, p)|^2, \\ \text{for} \quad 0 \le k \le \eta_1 N - 1 \quad \text{and} \\ \{0 \le p \le \eta_2 N - 1 : p/Q \in \mathbb{Z}\},\end{aligned} \tag{25}$$

where

$$\xi(k, p) = \frac{\sin\left[\frac{\pi}{Q}(k - p)\right]}{\sin\left[\frac{\pi}{N}(k - p - \eta_1 N)\right]}.$$

Again, note that when only one numerology occupies the whole spectrum (i.e., $Q = 1$), the I_{WSN} is zero as expected.

The signal-to-interference ratio (SIR) of p^{th} subcarrier of WSN due to $I_{\mathrm{WSN}}(k, p)$ is given by

$$\begin{aligned}\mathrm{SIR}_{\mathrm{WSN}}(p) &= \frac{\rho^{\mathrm{WSN}}(p)}{\sum_{k=0}^{\eta_1 N-1} I_{\mathrm{WSN}}(k, p)} \\ &= \frac{N \times M \times \rho^{\mathrm{WSN}}(p)}{\sum_{k=0}^{\eta_1 N-1} \rho^{\mathrm{NSN}}(k)|\xi(k, p)|^2}.\end{aligned} \tag{26}$$

Remark 1: From the INI expressions obtained in (18) and (25), we can deduce that the power ρ of the interfering numerology, spectrum sharing factor η, and the ratio $\Delta f_2/\Delta f_1 = N/M = Q$ of the multiplexed numerologies are the main factors affecting the amount of INI experienced by each numerology. One can easily note that if we increase Q (i.e., decrease M for a particular value of N), we minimize the product $N \times M$, resulting in a higher INI for both numerologies. This property was also observed by Zhang *et al.* in [4]. This suggests that for a given set of numerologies, system INI can be minimized by scheduling numerologies with minimum Q adjacent to each other.

Remark 2: A further analysis of (25) reveals that for some indices k of NSN subcarriers such that $k/Q \in \mathbb{Z}$, the term $\sin\left[\frac{\pi}{Q}(k - p)\right]$ in $\xi(k, p)$ is zero. This implies that NSN subcarriers occupying these particular set of indices (i.e., {indices $k : k/Q \in \mathbb{Z}$}) do not cause any interference to the WSN. In other words, the INI experienced by WSN is solely due to

the NSN subcarriers whose indices are not integer multiple of Q. This specific property of INI can be very useful in terms of scheduling. For instance, subcarriers of the NSN user with high power ρ can be scheduled to occupy these indices so that the WSN user does not suffer high INI from them.

Remark 3: The SIR expressions (19) and (26) show that any power offset between the two numerologies favors SIR performance of one numerology (with relatively higher power) and deteriorates the other (with low power). The fairer case is observed when the multiplexed numerologies have the same power (i.e., $\rho^{\text{NSN}} = \rho^{\text{WSN}}$), where SIR performance of both numerologies becomes independent of their powers. These analytical relationships provide the basis of the heuristic multi-numerology scheduling algorithms proposed in [18] and [19] where the authors suggest that numerologies with minimum power offsets should be scheduled adjacent to each other.

IV. INTER-NUMEROLOGY INTERFERENCE ANALYSIS FOR COMMON CP CONFIGURATION

While following the same derivation steps as detailed in Section III, here in this section we will only summarize the INI derivations for WSN and NSN.

A. INI FROM WSN TO NSN

The N-point FFT processing at the NSN receiver yields the interference $Y_{\text{INI}}(v)$ from WSN to v^{th} subcarrier of NSN as

$$\begin{aligned} Y_{\text{INI}}(v) &= \frac{1}{\sqrt{N}} \sum_{r=N_{\text{CP}}}^{N+N_{\text{CP}}-1} y^{C}_{\text{w}_c}(r) \text{e}^{-\frac{j2\pi}{N} rv} \\ &= \frac{1}{\sqrt{N}} \sum_{r=0}^{N-1} y^{C}_{\text{w}_c}(r+N_{\text{CP}}) \text{e}^{-\frac{j2\pi}{N}(r+N_{\text{CP}})v}. \end{aligned} \quad (27)$$

By using (8) and (5) and adopting the same step as in Appendix A and B, (27) can be simplified to

$$\begin{aligned} Y_{\text{INI}}(v) = \frac{1}{\sqrt{N \times M}} \sum_{q=0}^{Q-1} \sum_{k=0}^{\eta_2 N-1} X_{\text{w}_q}(\eta_1 M + k/Q) \\ \times \text{e}^{\frac{j2\pi}{N} N_{\text{CP}}(k-v+\eta_1 N)} \text{e}^{-\frac{j\pi}{N}(M-1)(k-v+\eta_1 N)} \cdot \zeta(k, v), \end{aligned} \quad (28)$$

where

$$\zeta(k, p) = \frac{\sin\left[\frac{\pi}{Q}(k-v)\right]}{\sin\left[\frac{\pi}{N}(k-v+\eta_1 N)\right]}.$$

Now, the INI power $I_{\text{NSN}}(k, v)$ from the k^{th} subcarrier of WSN to the v^{th} subcarrier of NSN is given as

$$\begin{aligned} I_{\text{NSN}}(k, v) = |Y_{\text{INI}}(k, v)|^2 = \frac{\rho^{\text{WSN}}(k)}{M^2} |\zeta(k, v)|^2, \\ \text{for} \quad 0 \le v \le \eta_1 N - 1 \quad \text{and} \\ \{0 \le k \le \eta_2 N - 1 : k/Q \in \mathbb{Z}\}. \end{aligned} \quad (29)$$

The SIR of the v^{th} subcarrier of NSN due to $I_{\text{NSN}}(k, v)$ is given as

$$\begin{aligned} \text{SIR}_{\text{NSN}}(v) &= \frac{\rho^{\text{NSN}}}{\sum_{k=0}^{\eta_2 N-1} I_{\text{NSN}}(k, v)} \\ &= \frac{M^2 \times \rho^{\text{NSN}}(v)}{\sum_{k=0}^{\eta_2 N-1} \rho^{\text{WSN}}(k) |\zeta(k, v)|^2}. \end{aligned} \quad (30)$$

B. INI FROM NSN TO WSN

Contrary to the previous case of WSN with individual CP where equalization is done for each of the Q-concatenated symbols, in this case, since all symbols share one CP, equalization is done over the whole block of Q WSN symbols. The equalized frequency domain signal is then converted back into the time domain where each symbol is demodulated through M-point FFT process. As we have mentioned before, further details concerning equalization with common CP can be found in [22] and [24]. Again, by considering perfect equalization, we calculate the interference Y_{INI} from NSN to WSN as

$$\begin{aligned} Y_{\text{INI}}(\eta_1 M + p/Q) \\ = \frac{1}{\sqrt{M}} \sum_{r=0}^{M-1} y_{\text{nr}}(r - qM) \text{e}^{-\frac{j2\pi}{N}(r-qM)(\eta_1 N+p)}. \end{aligned} \quad (31)$$

Substituting (3) into (31) and performing some simplifications similar to the ones used in Appendix A and B, an expression for the INI power, $I_{\text{WSN}}(k, p)$ from k^{th} subcarrier of NSN to p^{th} subcarrier of WSN can be found as

$$\begin{aligned} I_{\text{WSN}}(k, p) &= |Y_{\text{INI}}(k, \eta_1 M + p/Q)|^2 \\ &= \frac{\rho^{\text{NSN}}(k)}{N \times M} |\xi(k, p)|^2, \\ &\quad \text{for} \quad 0 \le k \le \eta_1 N - 1 \quad \text{and} \\ &\quad \{0 \le p \le \eta_2 N - 1 : p/Q \in \mathbb{Z}\}. \end{aligned} \quad (32)$$

One can notice from (25) and (32) that the INI power leaking from NSN to WSN for the individual and common CP cases is exactly the same. Therefore, the SIR performance in both cases is also the same, given by (26). In this regard, we can conclude that changing CP configuration affects INI distribution of NSN only.

One difference between the INI characteristics of the two investigated CP configurations is that the INI experienced by NSN for the individual CP is a function of CP_R, among other factors, while that is not the case with the common CP. This is intuitively plausible, as in the common CP configuration, no CP portion of WSN concatenated symbols overlaps with the symbol portion of the NSN (see Fig. 2).

Remark 4: Since the INI from NSN to WSN is the same for both individual and common CP cases, then the observation in Remark 2 holds for common CP as well. Furthermore, one can observe from (28) that, with the common CP configuration, the NSN subcarriers whose indices are integer multiple of Q (i.e., {indices $v : v/Q \in \mathbb{Z}$}) receive zero interference from WSN. Therefore, in conjunction with Remark 2,

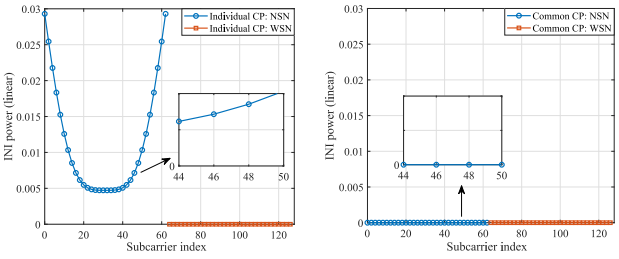

(a) Individual CP (b) Common CP

FIGURE 3. INI distribution when NSN user utilizes subcarrier indices which are integer multiples of Q (for $Q = 2$).

one can conclude that for common CP there is a set of NSN subcarriers (whose indices are integer multiple of Q) that neither cause nor receive interference from WSN. That is, this particular set of NSN subcarriers are fully orthogonal with WSN subcarriers.

Remarks 2 and 4 reveal a significant difference between individual and common CP configurations in terms of INI distribution and orthogonality. This difference is emphasized by Fig. 3, where we show that when only subcarriers whose indices are integer multiple of Q are used for NSN, multi-numerology system utilizing individual CP has a 'unidirectional-orthogonality' (i.e., zero INI from NSN to WSN only) whereas full orthogonality is achieved when common CP is used. In a nutshell, we can say that, although multi-numerology systems have been generally considered to be non-orthogonal, there is actually some degrees of orthogonality between some of the subcarriers of the multiplexed numerologies which has the potential of reshaping the ways in which we deal with the INI problem.

V. NUMERICAL RESULTS AND DISCUSSION

In this section we use Monte-Carlo simulations to evaluate the accuracy of the analytically derived INI expressions. A multi-numerology system utilizing CP-OFDM waveform with NSN and WSN numerologies equally sharing the available bandwidth (i.e., $\eta_1 = \eta_2 = 0.5$) is considered. Throughout the analysis, $\text{CP}_R = 1/16$, $N = 128$, and binary phase shift keying (BPSK) modulated symbols with unit power are used, unless otherwise specified. As we have observed from the analytic expression in the previous sections, the amount of INI experienced by each numerology in the system depends on the ratio Q of the subcarrier spacings of the multiplexed numerologies instead of the actual values of their subcarrier spacing. Therefore, we also consider evaluating performance of the system for different values of Q.

A. INI COMPARISON FOR INDIVIDUAL AND COMMON CP

Illustrated in Fig. 4 is the INI power experienced by each subcarrier of NSN and WSN for both individual and common CP configurations. As one could expect, the edge subcarriers of both numerologies are experiencing relatively higher INI compared to the middle subcarriers. This is due to the higher

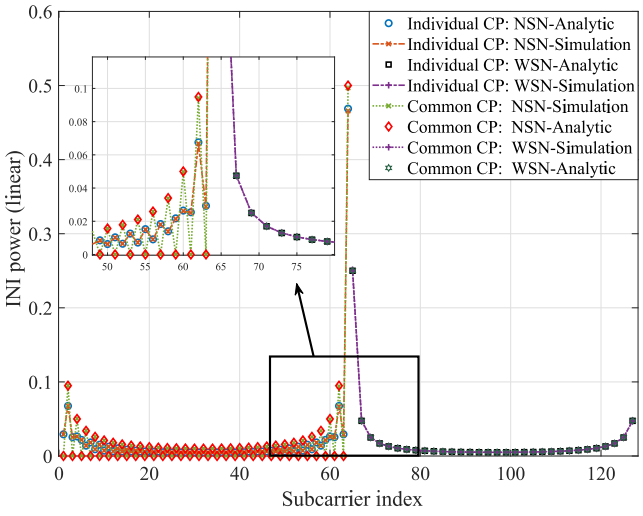

FIGURE 4. INI distribution on NSN and WSN subcarriers for individual and common CP configurations for Q = 2.

sidelobes of the adjacent numerology, whose effect abates as one moves away from the edges. As observed from the analytical expressions (25) and (32), the INI experienced by WSN is exactly the same for both CP configurations, and that agrees well with the simulation results shown in Fig. 4. The INI of NSN exhibits an interesting oscillatory behavior from one subcarrier to another. We reckon that this behavior is due to the discontinuities created at the boundaries of the Q-concatenating symbols of WSN. That is why, as it can be observed from Fig. V, this oscillation repeats itself after every Q subcarriers. This behavior is even more interesting when common CP configuration is used whereby NSN subcarriers occupying indices which are integer multiple of Q suffer zero INI from WSN as highlighted in Remark 4. In this case, one Q-th of all NSN subcarriers are free from INI problem. For example, for a multi-numerology system with 128 NSN subcarriers and $Q = 2, 64$ subcarriers will not be affected by INI from WSN. In essence, common CP localizes INI to only some of the subcarriers, making it capable of reducing complexity of the INI cancellation algorithms since the subcarriers with zero INI do not need to be included in the cancellation process. Similar kind of observation is reported in [13] for multi-numerology system utilizing UFMC waveform. This peculiar INI distribution exhibited by NSN can be of great advantage in some other practical aspects. For instance, with common CP configuration, pilot subcarriers for channel estimation or a reliability-sensitive user's subcarriers can be scheduled to those locations with zero INI to enhance their performances. Another critical thing to be noted from Fig. 4 is that the NSN subcarriers with non zero INI for the common CP case experience higher INI compared to when individual CP configuration is used. Therefore, the fact for the common CP configuration has an advantage of having a number of INI-free subcarriers comes at a cost of increased INI on the other subcarriers.

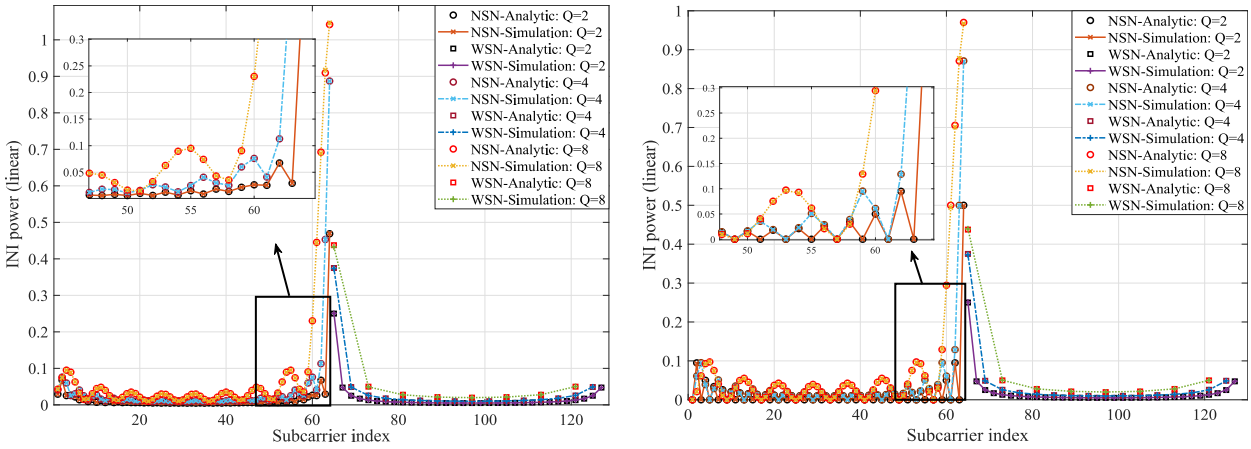

(a) Individual CP (b) Common CP

FIGURE 5. INI as a function of Q.

B. INI AS A FUNCTION OF SUBCARRIER SPACING RATIO (Q)

Here we investigate the effect of the ratio of different subcarrier spacings for the two numerologies. Fig. V shows INI distribution on each subcarrier of NSN and WSN for different values of Q. Here, from the definition of Q (i.e., $Q = \Delta f_2/\Delta f_1$), we fix Δf_1 at 15 kHz and change Δf_2 from 30 kHz, 60 kHz and 120 kHz. The INI each numerology receives seems to increase with the increase in Q. This is quite expected since the higher the Δf_2 the larger the sidelobes of the WSN that impart higher INI on NSN subcarriers. On the other hand, increasing Δf_2 widens the spectrum of the WSN and thus collects more interference from NSN.

Although the INI distribution among subcarriers of NSN and WSN with common and individual CP configurations is quite diverse, it is observed that, for a given Q, if $\rho^{\text{NSN}} = \rho^{\text{WSN}}$ (i.e., no power offset between the two numerologies), the average INI of NSN and WSN with common CP and WSN with individual CP are exactly the same. The average INI of NSN with individual CP is slightly different from the rest, as shown in Fig. 6. We interpret that this deviation is due to the dependency of the INI of NSN with individual CP on the CP_R (see (18)). That is, the CP portion of each of the Q-concatenated WSN symbols contributes to the INI experienced by NSN. In Fig. 6 we can see that the average INI of NSN with individual CP is smaller than the rest when $Q = 2$, and larger when $Q \geq 4$. The deviation is observed to be even more substantial with higher CP_R and higher Q.

C. EFFECT OF POWER OFFSET ON INI

Depending on the channel conditions and applications, users can have diverse power requirements, leading to power offset among them within the system. Power offset among the users utilizing the same numerology does not impose any threat on the performance of the system since the orthogonality is maintained. However, in the multi-numerology system, where INI exists, power offset between users utilizing

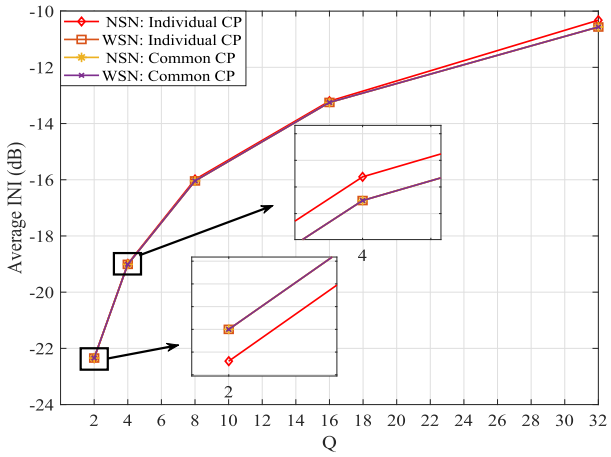

FIGURE 6. Average INI experienced by each numerology with individual and common CP for different values of Q.

different numerologies highly affects the SIR performance of the system [15]. Fig. 7 presents SIR performance of the multi-numerology system utilizing individual CP configuration as a function of power offset. The investigation is done for $Q = 2$, and two cases, $\rho^{\text{NSN}} > \rho^{\text{WSN}}$ and $\rho^{\text{WSN}} > \rho^{\text{NSN}}$, are considered. For each case, average SIR performance of each numerology as well as average SIR of the whole system are observed. It is clear from Fig. 7 that power offset favors the numerology with higher power and degrades performance of the other numerology with relatively lower power. This is obvious since numerology with higher power has stronger sidelobes whose interference to the adjacent numerology is more severe. We note from Fig. 7 that, the amount by which SIR of NSN is improved and that of WSN is degraded when $\rho^{\text{NSN}} > \rho^{\text{WSN}}$ is exactly the same as the amount by which SIR of WSN is improved and that of NSN is degraded when $\rho^{\text{WSN}} > \rho^{\text{NSN}}$. However, for a given power offset, average SIR of NSN is slightly larger than that of WSN. This is only because of using $Q = 2$. As we have discussed earlier, when $Q = 2$, average INI of NSN is slightly less compared to

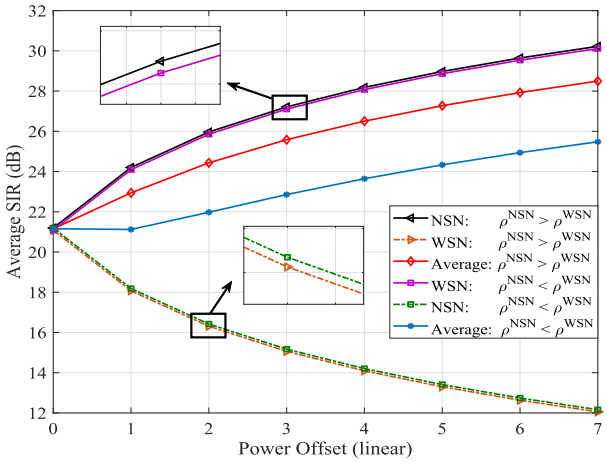

FIGURE 7. Average SIR of the multi-numerology system as a function of the power offset.

that of WSN (see Fig. 6). It is also observed from Fig. 7 that increasing power of one numerology relative to the other improves the overall average SIR of the system. However, this improvement is found to be dependent on which numerology has the higher power. The average system SIR is higher for the case with $\rho^{\text{NSN}} > \rho^{\text{WSN}}$ than $\rho^{\text{WSN}} > \rho^{\text{NSN}}$. The reason is that, for a given bandwidth, NSN has more subcarriers than WSN, making its effect on the average system SIR greater than that of WSN. Therefore, it is worth mentioning that the observed trend of the average system SIR is subjected to change when the two multiplexed numerologies do not share the available bandwidth equally (i.e., $\eta_1 \neq \eta_2$). We therefore understand that the overall SIR performance of the system is simultaneously affected by both power offset and bandwidth sharing factor, η.

From the above discussion it is evident that even though power offset among users of different numerologies may improve the overall system performance, it causes severe degradation in the performance of the numerology with relatively lower power. In order to favor both numerologies, it is more plausible to maintain the power offset between them as low as possible.

VI. CONCLUSION

The use of flexible numerology for different services of 5G has created the issue of numerology multiplexing and the consequent INI. This multiplexing requires alignment of the symbols corresponding to the different numerologies. In this paper, a relatively new alignment technique termed as common CP has been discussed in the light of 5G multi-numerology frame structure and the underlying problem of INI. In order to have a better grasp of the advantages of the common CP, the paper has presented a detailed analysis for both the conventional CP insertion technique (individual CP) and the common CP. The presented analysis reveals some interesting INI patterns for both CP configuration techniques. Although it has been considered that two different numerologies are by default non-orthogonal and thus interfere with each other, our analysis shows that, with the scalable multi-numerology structure of 5G, there is a degree of orthogonality that still exists between some of the narrow numerology subcarriers and the wide numerology subcarriers. It has been further shown that this degree of orthogonality can be increased through intelligent symbol design approaches such as common CP. These findings can dictate the way we implement scheduling and GB to minimize INI. In essence, it is intuitively understood that INI can be controlled or its effect can be significantly minimized through intelligent symbol design and scheduling, without resorting to spectrally inefficient techniques such as windowing and filtering. This study can prove instrumental in paving the way for utilization of alternative symbol design techniques for beyond 5G networks. Further analysis on INI minimization, cancellation or avoidance is left for future work. Investigation of the observed INI patterns with the common CP in the presence of channel impairments such as ISI, ICI and phase noise can also be considered for future research.

APPENDIX A SIMPLIFICATION OF (17)

Let us consider the first term of (17). If we rewrite indices r in terms of z such that $z = r - N_{\text{CP}}$, we have

$$\sum_{r=N_{\text{CP}}}^{M+M_{\text{CP}}-1} y_{\text{w}_0}(r)\mathrm{e}^{-j2\pi rv/N} = \sum_{z=0}^{M+M_{\text{CP}}-N_{\text{CP}}-1} y_{\text{w}_0}(z+N_{\text{CP}})\mathrm{e}^{-\frac{j2\pi}{N}v(z+N_{\text{CP}})}. \quad (33)$$

After evaluating the term $y_{\text{w}_0}(z+N_{\text{CP}})$ using (5), and rearranging the terms, (33) becomes

$$\begin{aligned} &= \frac{1}{\sqrt{M}} \sum_{z=0}^{M+M_{\text{CP}}-N_{\text{CP}}-1} \sum_{k=0}^{\eta_2 N-1} X_{\text{w}_0}(\eta_1 M + k/Q) \\ &\quad \times \mathrm{e}^{\frac{j2\pi}{N}(z+N_{\text{CP}})(k+\eta_1 N)}\mathrm{e}^{-\frac{j2\pi}{N}v(z+N_{\text{CP}})} \\ &= \frac{1}{\sqrt{M}} \sum_{k=0}^{\eta_2 N-1} X_{\text{w}_0}(\eta_1 M + k/Q)\mathrm{e}^{\frac{j2\pi}{N}N_{\text{CP}}(k-v+\eta_1 N)} \\ &\quad \times \sum_{z=0}^{M+M_{\text{CP}}-N_{\text{CP}}-1} \mathrm{e}^{-\frac{j2\pi}{N}z(k-v+\eta_1 N)}. \end{aligned} \quad (34)$$

Applying the formula for the sum of finite geometric series $\left(\text{i.e., } \sum_{t=0}^{T} \mathrm{a}^t = (1-a^{T+1})/(1-a)\right)$ on the term with summation over z-indices gives

$$\begin{aligned} &= \frac{1}{\sqrt{M}} \sum_{k=0}^{\eta_2 N-1} X_{\text{w}_0}(\eta_1 M + k/Q)\mathrm{e}^{\frac{j2\pi}{N}N_{\text{CP}}(k-v+\eta_1 N)} \\ &\quad \times \frac{1-\mathrm{e}^{\frac{j2\pi}{N}(M+M_{\text{CP}}-N_{\text{CP}})(k-v+\eta_1 N)}}{1-\mathrm{e}^{\frac{j2\pi}{N}(k-v+\eta_1 N)}}. \end{aligned} \quad (35)$$

By using Euler's identity $\sin(\theta) = (e^{j\theta} - e^{-j\theta})/2j$ on the last term and simplifying, (35) consequently becomes

$$= \frac{1}{\sqrt{M}} \sum_{k=0}^{\eta_2 N-1} X_{w_0}(\eta_1 M + k/Q) e^{\frac{j2\pi}{N} N_{CP}(k-v+\eta_1 N)} \times e^{\frac{j\pi}{N}(M+M_{CP}-N_{CP}-1)(k-v+\eta_1 N)} \times \frac{\sin\left[\frac{\pi}{N}(M+M_{CP}-N_{CP})(k-v)\right]}{\sin\left[\frac{\pi}{N}(k-v+\eta_1 N)\right]}. \quad (36)$$

Again, by using (5) and following the same steps as above, the second term of (17) can be expressed as

$$\sum_{r=0}^{M+M_{CP}-1} \sum_{q=1}^{Q-1} y_{w_q}(r - q(M+M_{CP})) e^{\frac{-j2\pi}{N} v(r-q(M+M_{CP}))} = \sum_{q=1}^{Q-1} \frac{1}{\sqrt{M}} \sum_{k=0}^{\eta_2 N-1} X_{w_q}(\eta_1 M + k/Q) \times e^{-\frac{j2\pi}{N}(M+M_{CP})(k-v+\eta_1 N)} e^{\frac{j\pi}{N}(M+M_{CP}-1)(k-v+\eta_1 N)} \times \frac{\sin\left[\frac{\pi}{N}(M+M_{CP})(k-v)\right]}{\sin\left[\frac{\pi}{N}(k-v+\eta_1 N)\right]}. \quad (37)$$

APPENDIX B SIMPLIFICATION OF (24)

Substituting (3) into (24), we have

$$\begin{aligned} Y_{INI}(\eta_1 M + p/Q) &= \frac{1}{\sqrt{M \times N}} \sum_{r=0}^{M-1} \sum_{k=0}^{\eta_1 N-1} X_{nr}(k) e^{\frac{j2\pi}{N} k(r+M_{CP}-q(M+M_{CP}))} \times e^{-\frac{j2\pi}{M}(r+M_{CP})(\eta_1 M+p/Q)} \\ &= \frac{1}{\sqrt{M \times N}} \sum_{k=0}^{\eta_1 N-1} X_{nr}(k) e^{-\frac{j2\pi}{N} k(M_{CP}-q(M+M_{CP}))} \times e^{-\frac{j2\pi}{M}(M_{CP}(\eta_1 M+p/Q))} \sum_{r=0}^{M-1} e^{-\frac{j2\pi}{N} r(k-p-\eta_1 N)} \\ &\overset{(a)}{=} \frac{1}{\sqrt{M \times N}} \sum_{k=0}^{\eta_1 N-1} X_{nr}(k) e^{-\frac{j2\pi}{N} k(M_{CP}-q(M+M_{CP}))} \times e^{-\frac{j2\pi}{M}(M_{CP}(\eta_1 M+p/Q))} \times \frac{1 - e^{\frac{j2\pi}{N} M(k-p-\eta_1 N)}}{1 - e^{\frac{j2\pi}{N}(k-p-\eta_1 N)}} \\ &\overset{(b)}{=} \frac{1}{\sqrt{M \times N}} \sum_{k=0}^{\eta_1 N-1} X_{nr}(k) e^{-\frac{j2\pi}{N} k(M_{CP}-q(M+M_{CP}))} \times e^{-\frac{j2\pi}{M}(M_{CP}(\eta_1 M+p/Q))} e^{-\frac{j2\pi}{N}(M-1)(k-p-\eta_1 N)} \times \frac{\sin\left[\frac{\pi}{Q}(k-p)\right]}{\sin\left[\frac{\pi}{N}(k-p-\eta_1 N)\right]}, \end{aligned} \quad (38)$$

where the equalities (a) and (b) again follow after employing the formula for the sum of a finite geometric series on the summation over r-indices, and Euler's formula, respectively, as detailed in Appendix A.

REFERENCES

[1] *5G Vision—The 5G Infrastructure Public Private Partnership: The Next Generation of Communication Networks and Services*, 5G Infrastruct. PPP Assoc., Eur. Commission, Brussels, Belgium, Feb. 2015.

[2] A. A. Zaidi, R. Baldemair, H. Tullberg, H. Bjorkegren, L. Sundstrom, J. Medbo, C. Kilinc, and I. Da Silva, "Waveform and numerology to support 5G services and requirements," *IEEE Commun. Mag.*, vol. 54, no. 11, pp. 90–98, Nov. 2016.

[3] E. Dahlman, S. Parkvall, and J. Skold, *5G NR: The Next Generation Wireless Access Technology*. New York, NY, USA: Academic, 2018.

[4] X. Zhang, L. Zhang, P. Xiao, D. Ma, J. Wei, and Y. Xin, "Mixed numerologies interference analysis and inter-numerology interference cancellation for windowed OFDM systems," *IEEE Trans. Veh. Tech.*, vol. 67, no. 8, pp. 7047–7061, Apr. 2018.

[5] X. Zhang, L. Chen, J. Qiu, and J. Abdoli, "On the waveform for 5G," *IEEE Commun. Mag.*, vol. 54, no. 11, pp. 74–80, Nov. 2016.

[6] R. Gerzaguet, N. Bartzoudis, L. G. Baltar, V. Berg, J.-B. Doré, D. Kténas, O. Font-Bach, X. Mestre, M. Payaró, M. Färber, and K. Roth, "The 5G candidate waveform race: A comparison of complexity and performance," *EURASIP J. Wireless Commun. Netw.*, vol. 2017, no. 1, p. 13, 2017.

[7] Z. E. Ankarali, B. Peköz, and H. Arslan, "Flexible radio access beyond 5G: A future projection on waveform, numerology, and frame design principles," *IEEE Access*, vol. 5, pp. 18295–18309, 2017.

[8] A. Yazar and H. Arslan, "A flexibility metric and optimization methods for mixed numerologies in 5G and beyond," *IEEE Access*, vol. 6, pp. 3755–3764, 2018.

[9] "5G waveform candidates," Rohde Schwarz, Munich, Germany, Appl. Note 1MA271-0e, Jun. 2016.

[10] *NR; Physical Channels and Modulation (Release 15)*, document TS 38.211, Version 15.1.0, 3GPP, Apr. 2018.

[11] J. Vihriälä, A. A. Zaidi, V. Venkatasubramanian, N. He, E. Tiirola, J. Medbo, E. Lähetkangas, K. Werner, K. Pajukoski, A. Cedergren, and R. Baldemair, "Numerology and frame structure for 5G radio access," in *Proc. IEEE 27th Annu. Int. Symp. Pers., Indoor, Mobile Radio Commun. (PIMRC)*, Valencia, Spain, Sep. 2016, pp. 1–5.

[12] J. Sachs, G. Wikstrom, T. Dudda, R. Baldemair, and K. Kittichokechai, "5G radio network design for ultra-reliable low-latency communication," *IEEE Netw.*, vol. 32, no. 2, pp. 24–31, Mar./Apr. 2018.

[13] L. Zhang, A. Ijaz, P. Xiao, A. Quddus, and R. Tafazolli, "Subband filtered multi-carrier systems for multi-service wireless communications," *IEEE Trans. Wireless Commun.*, vol. 16, no. 3, pp. 1893–1907, Mar. 2017.

[14] L. Zhang, A. Ijaz, P. Xiao, A. Quddus, and R. Tafazolli, "Single-rate and multi-rate multi-service systems for next generation and beyond communications," in *Proc. IEEE 27th Annu. Int. Symp. Pers., Indoor, Mobile Radio Commun. (PIMRC)*, Valencia, Spain, Sep. 2016, pp. 1–6.

[15] A. B. Kihero, M. S. J. Solaija, A. Yazar, and H. Arslan, "Inter-numerology interference analysis for 5G and beyond," in *Proc. IEEE Globecom Workshops (GC Wkshps)*, Dec. 2018, pp. 1–6.

[16] L. Zhang, A. Ijaz, J. Mao, P. Xiao, and R. Tafazolli, "Multi-service signal multiplexing and isolation for physical-layer network slicing (PNS)," in *Proc. IEEE 86th Veh. Technol. Conf. (VTC-Fall)*, Sep. 2017, pp. 1–6.

[17] S. Eldessoki, D. Wieruch, and B. Holfeld, "Impact of waveforms on coexistence of mixed numerologies in 5G URLLC networks," in *Proc. Int. ITG Workshop Smart Antennas (WSA)*, Berlin, Germany, 2017, pp. 1–6.

[18] A. F. Demir and H. Arslan, "The impact of adaptive guards for 5G and beyond," in *Proc. IEEE Annu. Int. Symp. Pers., Indoor, Mobile Radio Commun. (PIMRC)*, Montreal, QC, Canada, Oct. 2017, pp. 1–5.

[19] A. Yazar and H. Arslan, "Flexible multi-numerology systems for 5G new radio," *J. Mobile Multimedia*, vol. 14, no. 4, pp. 367–394, Oct. 2018.

[20] J. Choi, B. Kim, K. Lee, and D. Hong, "A transceiver design for spectrum sharing in mixed numerology environments," *IEEE Trans. Wireless Commun.*, vol. 18, no. 5, pp. 2707–2721, May 2019.

[21] T. Levanen, J. Pirskanen, K. Pajukoski, M. Renfors, and M. Valkama, "Transparent Tx and Rx waveform processing for 5G new radio mobile communications," *IEEE Wireless Commun.*, vol. 26, no. 1, pp. 128–136, Feb. 2019.

[22] X. Wang, Y. Wu, and J-Y. Chouinard, "On the comparison between conventional OFDM and MSE-OFDM systems," in *Proc. IEEE Global Telecommun. Conf. (GLOBECOM)*, San Francisco, CA, USA, vol. 1, Dec. 2003, pp. 35–39.

[23] J.-Y. Chouinard, X. Wang, and Y. Wu, "MSE-OFDM: A new OFDM transmission technique with improved system performance," in *Proc. IEEE Int. Conf. Acoust., Speech, Signal Process. (ICASSP)*, Philadelphia, PA, USA, vol. 3, Mar. 2005, pp. 865–868.

[24] M. Nemati and H. Arslan, "Low ICI symbol boundary alignment for 5G numerology design," *IEEE Access*, vol. 6, pp. 2356–2366, 2018.

[25] A. T. Abusabah and H. Arslan, "NOMA for multinumerology OFDM systems," *Wireless Commun. Mobile Comput.*, vol. 2018, May 2018, Art. no. 8514314.

[26] T. Hwang, C. Yang, G. Wu, S. Li, and G. Y. Li, "OFDM and its wireless applications: A survey," *IEEE Trans. Veh. Technol.*, vol. 58, no. 4, pp. 1673–1694, May 2009.

ABUU B. KIHERO received the B.S. degree in electronics engineering from Gebze Technical University, Kocaeli, Turkey, in 2015, and the M.S. degree in electrical, electronics, and cyber systems from Istanbul Medipol University, Istanbul, Turkey, in 2018, and the Ph.D. degree in wireless communication technologies from Istanbul Medipol University. He is currently a Research Assistant with the Communication, Signal Processing, and Networking Center, Istanbul Medipol University. His research interests include wireless channel modeling and emulation, interference modeling, and coordinated multipoint (COMP) for 5G and beyond wireless systems.

MUHAMMAD SOHAIB J. SOLAIJA (S'16) received the B.E. and M.Sc. degrees in electrical engineering from the National University of Science and Technology, Islamabad, Pakistan, in 2014 and 2017, respectively. He is currently pursuing the Ph.D. degree with the Communications, Signal Processing, and Networking Center, Istanbul Medipol University, Turkey. His research interests include interference modeling, and coordinated multipoint implementation for 5G and beyond wireless systems.

HÜSEYIN ARSLAN (S'95–M'98–SM'04–F'15) received the B.S. degree from Middle East Technical University (METU), Ankara, Turkey, in 1992, and the M.S. and Ph.D. degrees from Southern Methodist University (SMU), Dallas, TX, USA, in 1994 and 1998, respectively. From January 1998 to August 2002, he was with the Research Group, Ericsson Inc., NC, USA, where he was involved in several projects related to 2G and 3G wireless communication systems. Since August 2002, he has been with the Electrical Engineering Department, University of South Florida, Tampa, FL, USA. Also, he has been the Dean of the College of Engineering and Natural Sciences, Istanbul Medipol University, since 2014. In addition, he has worked as a part-time Consultant for various companies and institutions including Anritsu Company, Morgan Hill, CA, USA, and The Scientific and Technological Research Council of Turkey (TUBITAK). His current research interests include physical layer security, mmWave communications, small cells, multicarrier wireless technologies, co-existence issues on heterogeneous networks, aeronautical (high altitude platform) communications and in vivo channel modeling, and system design.